Magnetization dynamics in dilute $Pd_{1-x}Fe_x$ thin films and patterned microstructures considered for superconducting electronics

I. A. Golovchanskiy,[1,2] V. V. Bolginov,[2,3] N. N. Abramov,[2] V. S. Stolyarov,[1,3,4] A. Ben Hamida,[2] V. I. Chichkov,[2] D. Roditchev,[5] and V. V. Ryazanov[1,2,3,4]
[1]*Moscow Institute of Physics and Technology, State University, 9 Institutskiy per., Dolgoprudny, Moscow Region 141700, Russia*
[2]*National University of Science and Technology MISIS, 4 Leninsky Prospect., Moscow 119049, Russia*
[3]*Institute of Solid State Physics (ISSP RAS), Chernogolovka, Moscow Region 142432, Russia*
[4]*Solid State Physics Department, Kazan Federal University Kazan 420008, Russia*
[5]*Laboratoire de Physique et d'Etudes des Materiaux, ESPCI-ParisTech, CNRS and UPMC Univ Paris 6 - UMR 8213, 10 rue Vauquelin, Paris 75005, France*

(Received 13 June 2016; accepted 11 October 2016; published online 26 October 2016)

Motivated by recent burst of applications of ferromagnetic layers in superconducting digital and quantum elements, we study the magnetism of thin films and patterned microstructures of $Pd_{0.99}Fe_{0.01}$. In this diluted ferromagnetic system, a high-sensitivity ferromagnetic resonance (FMR) experiment reveals spectroscopic signatures of re-magnetization and enables the estimation of the saturation magnetization, the anisotropy field, and the Gilbert damping constant. The detailed analysis of FMR spectra links the observed unexpectedly high reduced anisotropy field (0.06–0.14) with the internal anisotropy, points towards a cluster nature of the ferromagnetism, and allows estimating characteristic time scale for magnetization dynamics in Pd-Fe based cryogenic memory elements to $(3-5)\times10^{-9}$ s. *Published by AIP Publishing*. [http://dx.doi.org/10.1063/1.4965991]

I. INTRODUCTION

Since very recently, weak ferromagnetic layers with low coercivity regain strong practical interest due to their integration in various superconductor-ferromagnet-superconductor (SFS) Josephson spintronic elements[1–13] and superconducting ultra-fast electronic devices.[14,15] Characterized by the low magnetic moment, Curie temperature, and exchange field, two major candidates, Cu-Ni and Pd-Fe alloys, are currently considered for SFS applications. Historically, a weak ferromagnetic Cu-Ni alloy was the first used in Nb-CuNi-Nb SFS junctions to demonstrate the Josephson supercurrent flow through the ferromagnetic barrier as well as the inversion of the current-phase relation (π-state).[13,16,17] However, due to their stable magnetic domain structure (high coercive field) and out-of-plane magnetic anisotropy, the Cu-Ni alloys are useful only for fabrication of the superconducting phase inverters with constant phase shifts useful for digital[16–19] and quantum[17,20,21] logic. In contrast, Pd-Fe alloys with a low Fe content exhibit an in-plane anisotropy and small coercive field that makes them perfect candidates for novel Josephson cryogenic magnetic memory elements.[8–11] In these devices, the value of the critical Josephson current is defined by the in-plane magnetic flux including the magnetization orientation and is governed by the magnetic history of the ferromagnetic layer.

Pd-Fe alloys belong to a long time known class of weak ferromagnets composed of palladium or platinum doped by transition metals (i.e., Fe, Co, and Ni).[22–24] Since Pd is on the verge of magnetic instability, the Fe concentration as low as 0.005 at. % is sufficient to trigger the spontaneous magnetization of the entire matrix at a mK-range Curie temperature.[25] At that concentration, a "giant" effective magnetic moment per Fe atom up to $\sim10\,\mu_B$ emerges.[23,24] This "giant" moment arises from the magnetic polarization of the Pd or Pt clouds of atoms in the vicinity of 3d atoms[22,26] or clusters[27] and subsequent percolation of polarized clouds.[23] While for lower Fe concentrations, Pd-Fe behaves as a spin glass,[28] for higher concentrations the magnetization and the Curie temperature increase monotonically with increasing Fe concentration up to 400 K for 20 at. % of Fe.[29] Owing to their soft ferromagnetism and tunable Curie temperature, Pd-Fe alloys are widely used in various applications or experiments where a soft ferromagnet with tunable Curie temperatures below room temperature is required (see Ref. 29 and references within).

Since $Pd_{0.99}Fe_{0.01}$ based SFS Josephson junctions are considered as promising elements of fast cryogenic memories, the knowledge of dynamic ferromagnetic properties of thin Pd-Fe layers is required. Indeed, one of the key issues of any memory element is the operating speed, i.e., a switching period of the F-barrier between "0" and "1" magnetic states. The ferromagnetic resonance (FMR) experiment we report in this paper provides the necessary basic knowledge on dynamical properties of $Pd_{0.99}Fe_{0.01}$ ferromagnets, including the estimation of the characteristic response time of the F-layer or, for example, the time scale for microwave-assisted magnetization switching period[30,31] which can be associated with the corresponding zero-field ferromagnetic resonance frequency. Yet, FMR investigation of $Pd_{0.99}Fe_{0.01}$ thin films is a challenging experimental task due to a very weak FMR absorption signal and low Curie temperature. This is why till now, to our best knowledge, the FMR experiments were limited to the studies of relatively thick[32] or Fe-rich Pd-Fe films.[33] Owing to the substantial improvements of the FMR technique, we report here a high-sensitive measurement of the FMR

spectrum of the $Pd_{0.99}Fe_{0.01}$ 100-nm thick film, its comparison with the one of the conventional ferromagnetic thin films of Permalloy (Py). Finally, we derive essential static and dynamic magnetic parameters of the studied $Pd_{0.99}Fe_{0.01}$ films from the FMR spectra.

II. EXPERIMENTAL DETAILS

The FMR study employing microwave signal (MW) absorption by Pd-Fe thin films was conceived following Refs. 34 and 35. The technique is based on the interaction of the microwave signal transmitted through a coplanar wave guide (CPW) with the ferromagnetic sample placed in close proximity.

A schematic illustration of the experiment including the sample design is shown in Fig. 1(a). The studied FM film (shown in red) is deposited on the central stripe of the CPW formed on the Si substrate. The FM film couples to the RF magnetic field of the CPW and causes resonant losses and phase shift at FMR frequency. The experimental chip was installed in a copper sample holder and wire bonded to PCB with RF connectors. A thermometer and a heater were screwed directly to the holder for precision temperature control. To study the RF response of the film at various temperatures and magnetic fields, the holder is placed in a homemade superconducting magnet inside a dry closed-cycle cryostat with Joule - Thompson He4 stage (Oxford Instruments Triton, base temperature 1.2 K); bias magnetic field (green arrow in Fig. 1(a)) is oriented in-plane and parallel to the direction of the MW propagation, i.e., perpendicular to the RF field. The setup enables measuring the ferromagnetic response of pristine and micro-patterned films at different temperatures (1.2–50) K and magnetic fields up to 1 T. The response of the system is studied by analyzing the transmitted MW signal S_{21} by vector network analyzer (VNA) Rohde & Schwarz ZVB20.

To enable the measurement of the weak FMR response of diluted thin FM films, several improvements of the technique have been implemented as compared to standard approaches,[34,35] in order to enhance its overall sensitivity. First, the superconducting Nb CPWs were employed instead of widely used normal metal (Cu) CPWs. The superconducting Nb CPW has improved characteristics as compared to Cu-CPW thanks to reduced resistive losses that mask the weak response of the FM film. Nb CPWs were fabricated using laser lithography and plasma-chemical etching techniques in $CF_4 + O_2$ out of Nb films deposited onto the Si substrate. Second, the thickness of the CPW was reduced to confine the AC magnetic fields at the surface and improve the inductive coupling with the FM sample. The optimum design was obtained with a 150 μm wide and 200 nm thick central stripe of the CPW; the use of 85 μm gaps yields 50 Ω impedance. Third, the FM films were deposited directly on top of the Nb transmission line, by successive magnetron sputtering and lift-off, instead of using a so-called "flip-chip" technique (when the FM film is flipped onto the measurement transmission line). This approach maximizes both the uniformity of the AC-field in the ferromagnet[35] and the inductive coupling of the FM film to the MW. Finally, the length of CPW was maximized by folding the CPW into a 60 mm long meander. It allows coupling a large number of FM structures to the CPW and maximizing the signal-to-noise ratio. The folded design permits to keep reasonably compact the lateral dimensions (15×15 mm) of the whole test chip.

$Pd_{0.99}Fe_{0.01}$ thin films were deposited directly onto Nb CPWs using argon RF-sputtering of the $Pd_{0.99}Fe_{0.01}$ alloy target. During the deposition, the argon pressure and deposition rate were 1.5×10^{-2} mBar and 1.5 Å/s, respectively. The base pressure in the growth chamber prior deposition was 2×10^{-6} mBar. Fig. 1(b) demonstrates a typical topographic STM image of the surface of the $Pd_{0.99}Fe_{0.01}$ film that witnesses on a peculiar film morphology. A description of the STM imaging of *in-situ* cleaved *ex-situ* elaborated films can be found elsewhere.[36] The STM image shows a disordered yet dense arrangement of $\sim 5-10$ nm grains and of darker grain-free regions. The latter have a typical size of $\sim 10-30$ nm; they are ~ 100 nm distant from each other. The observed morphology corresponds well to the expected magnetic structure of $Pd_{0.99}Fe_{0.01}$/Nb. As discussed earlier,[27] the magnetic moment of dilute $Pd_{0.99}Fe_{0.01}$ thin films deposited on Nb is

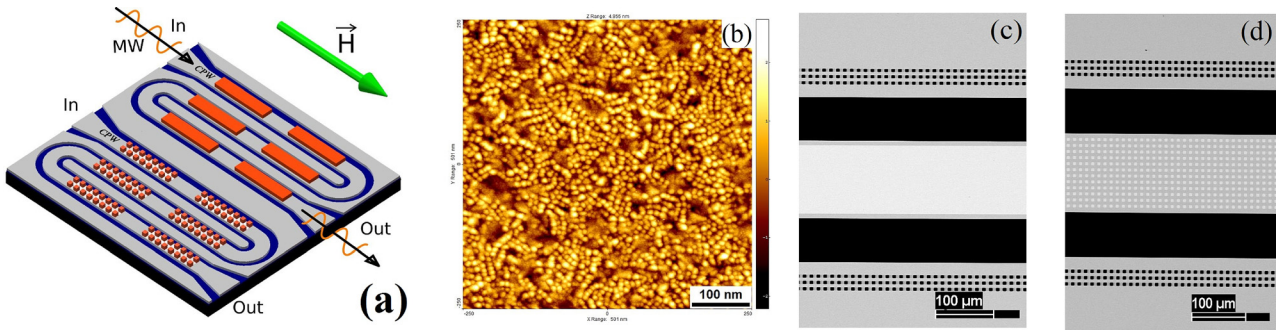

FIG. 1. (a) Schematic illustration of the sample design for FMR measurements. Patterned Pd-Fe films (in red) are placed onto a 50 Ω coplanar waveguide (CPW) made of Nb (in grey-blue); gaps of the CPW are shown in dark blue. Black and green arrows show, respectively, the direction of propagation of the microwave signal and the direction of the external magnetic field (see precisions in the text). (b) High resolution constant current STM image of the in-vacuum cleaved surface of 40 nm $Pd_{0.99}Fe_{0.01}$ evidencing a granular structure of the film. The typical apparent grain size is ≈5 nm. Depleted regions showing no granular structure are also present. Scanning conditions: bias voltage 787 mV, tunnel current 38 pA, pressure at STM chamber 1.2×10^{-10} mbar, and temperature 1.3 K. (c) SEM image of the coplanar waveguide with the ferromagnetic thin-film bar sample. (d) SEM image of the coplanar waveguide with the ferromagnetic thin-film array sample.

controlled by Fe-rich nano-clusters of at least ~10 nm and magnetic moment per Fe ion of ~3.7 μ_B which is close to 4 μ_B for the Pd_3Fe compound.[37] The Curie temperature shows a strong dependence on film thickness[8,27,38] and disappears for thickness below 10 nm.[8,27,39] The existence of the thickness threshold for spontaneous magnetization can be related to the percolation transition in granular films.

On each test chip (Fig. 1(a)), two types of $Pd_{0.99}Fe_{0.01}$ samples were patterned: a series of 1100 × 140 μm large rectangles with 200 μm spacing (referred to as bar sample, Fig. 1(c)) and arrays of small 5 × 5 μm squares of 10 × 10 μm array period (referred to as array sample, Fig. 1(d)). The FMR spectra of bar samples allow us to estimate basic magnetic properties of corresponding thin films while FMR spectra of array samples enable a deeper insight into the magnetization dynamics of $Pd_{0.99}Fe_{0.01}$ of a lateral size typical for SFS junctions. The same was done for Py samples used for the sensitivity tests and calibration. The Py thin film samples were deposited using the same deposition setup but in the presence of in-plane magnetic field, which induces anisotropy field along the CPW and accordingly along the applied magnetic field.

Prior to the actual FMR measurement, normalization of transmission was performed at bias field 150 kA/m, when the FMR frequency is pushed far above the measurement range, to eliminate any field independent background since the FMR response is relatively weak.

Derivation of FMR frequency dependence on applied magnetic field was performed using a complex susceptibility response for a thin film magnetized to saturation as discussed in Ref. 40.

III. CALIBRATION AND SENSITIVITY OF FMR SETUP

The calibration and the sensitivity tests of our FMR measurement setup were performed using Py samples, which are well-known model magnetic materials. Fig. 2(a) shows an FMR spectrum of a 100 nm Py thin film bar sample measured at 2 K. The DC magnetic field was swept from +1.8 $\times 10^4$ to -1.8×10^4 A/m in order to observe all FMR spectral features related to re-magnetization. The discontinuity observed in the FMR spectrum of the bar sample demonstrates the re-magnetization to occur at $H \simeq 1.5 \times 10^3$ A/m. The anisotropy field (H_a) and the magnetization saturation (M_s) can be derived from the dependence of FMR frequency f_r on applied magnetic field H employing the Kittel formula for thin films with in-plane magnetization in the absence of a perpendicular or surface anisotropy[34,41]

$$(2\pi f_r/\gamma)^2 = (H + H_a)(H + H_a + M_s), \qquad (1)$$

where $\gamma = 2.21 \times 10^5$ m/A/s is the gyromagnetic ratio.

The fit of the FMR dependence on the applied magnetic field using Eq. (1) (the fitted $f_r(H)$ curve is presented as a yellow dashed line in Fig. 2(a)) yields the saturation magnetization $M_s \simeq 9.2 \times 10^5$ A/m and the anisotropy field $H_a \simeq 2.9 \times 10^3$ A/m. These are typical values for Permalloy thin films.[42–44] A relatively high anisotropy field is justified

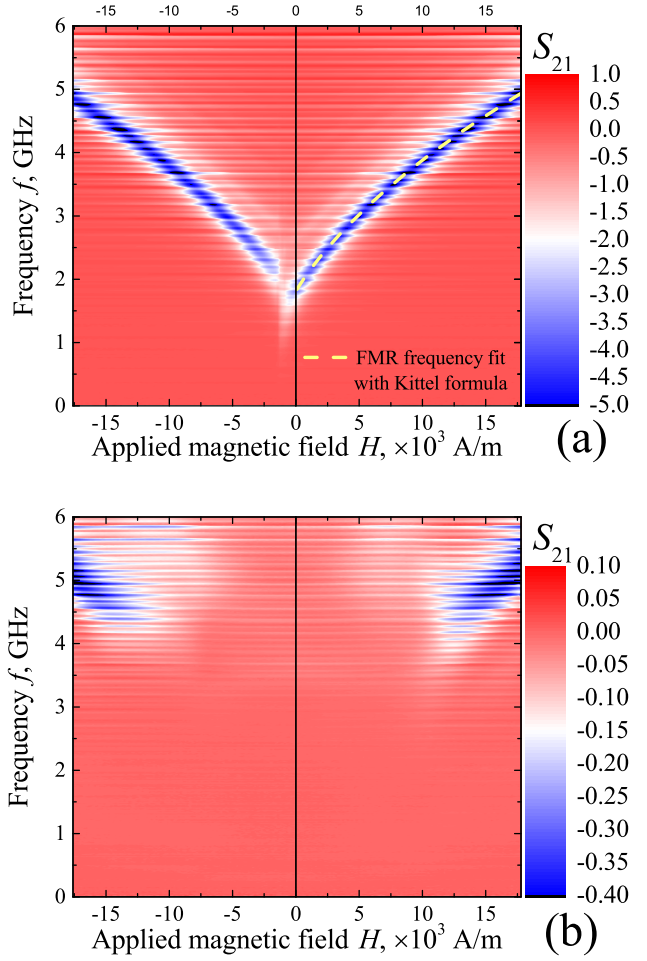

FIG. 2. Colour-coded absorption FMR spectra in the frequency - field coordinates acquired for Py films: (a) bar sample and (b) array sample. The red-blue colour palette represents the relative MW absorption due to FM films in dB. Yellow dashed line—the best fit using Kittel expression, Eq. (1) (see in the text).

by the shape anisotropy of Py thin film bar samples,[45,46] as well as by the film growth induced internal anisotropy.

In Fig. 2(b), we present a FMR spectrum of the Py array sample. At high enough magnetic fields, the general shape of the FMR absorption spectrum displayed in the frequency-field coordinates is very similar to the one of Py bar samples, Fig. 2(a); the characteristic values are also very close, $f_r(1.75 \times 10^4$ A/m $) \simeq 5$ GHz. Remarkably, the FMR signal disappears completely at the magnetic fields below $H \approx 10^4$ A/m, indicating a transition of Py array samples from the magnetized to the vortex state induced by H_{AC}. The transition to the vortex state implies the dominance of the demagnetizing field over the exchange field for the 5 × 5 μm^2 array Py film.

Finally, we compared the amplitude of the measured FMR signal in our experiment with the results available in the literature. In our case, the MW absorption for the Py film was >5 dB at the resonance, i.e., by one order of magnitude higher than in the reported FMR experiments provided on Py films of the same thickness (see, for example, Ref. 39). The enhanced sensitivity of our experimental setup is very important in view of FMR measurements of thin and weak ferromagnetic Pd-Fe films.

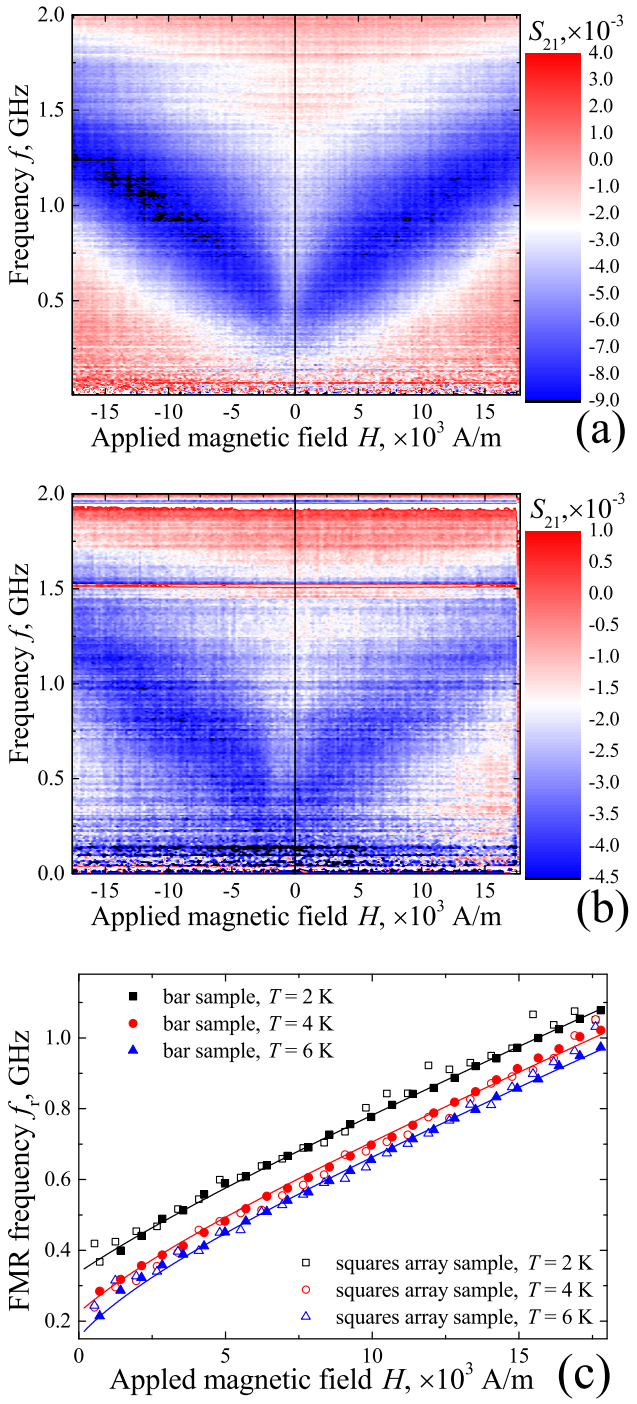

FIG. 3. Absorption FMR spectra of $Pd_{0.99}Fe_{0.01}$ films: (a) bar sample and (b) array sample. (c) Evolution of the FMR frequency with DC-magnetic field measured at different temperatures (symbols). Lines best fit with the Kittel formula (Eq. (1)).

IV. FERROMAGNETIC RESONANCE OF $Pd_{0.99}Fe_{0.01}$ THIN FILM SAMPLES

Figs. 3(a) and 3(b) show, respectively, the FMR spectrum of the 100 nm-thick $Pd_{0.99}Fe_{0.01}$ bar sample and that of the array sample, both measured at 2 K. In contrast to the case of Py, the FMR spectrum of $Pd_{0.99}Fe_{0.01}$ is continuous for both types of samples. This witnesses for a smooth re-magnetization process with no sign of a vortex phase. The continuous spectrum of the array sample might indicate a dominance of the exchange field over the demagnetizing field, or a large anisotropy field, since the $5 \times 5\,\mu$m square arrays do not transit into a vortex state at $H \to 0$. The smooth evolution of the FMR spectrum along with the presence of the FMR absorption at $H = 0$ observed in array samples makes thin Pd-Fe microstructures suitable for designing SFS magnetic memory elements.

The maximum FMR absorption signal measured on the 100 nm-thick bar sample was $\sim 10^{-2}$ dB; it was $\sim 3 \times 10^{-3}$ dB for the 100 nm-thick array sample. The weak MW absorption signal and a low quality factor of the FMR ($\sim$2) complicate the precise determination of the FMR frequency and the frequency bandwidth, allowing only estimations of M_s and H_a.

We have to note here that we studied the samples with thickness varying from 30 nm (typical thickness required for Josephson spintronic applications) to 500 nm (bulky films). However, a very weak FMR absorption and low signal-to-noise ratio made impossible a quantitative analysis of the FMR spectra of samples thinner than $\approx$100 nm. On the other side, FMR spectra of all thicker $Pd_{0.99}Fe_{0.01}$ samples did not show any qualitative or quantitative difference compared to the one of 100 nm thick one (Fig. 3), except the amplitude of the FMR absorption, which is simply proportional to the film thickness. Thus, below we limit the discussion to 100 nm-thick $Pd_{0.99}Fe_{0.01}$ samples.

Fig. 3(c) presents $f_r(H)$ curves derived from the FMR spectra measured on 100 nm-thick $Pd_{0.99}Fe_{0.01}$ at different temperatures (symbols). The lines are $f_r(H)$ fits using Eq. (1). For the bar sample, the fits yield weakly temperature dependent saturation magnetization: $M_s \sim 2.5 \times 10^4$ A/m, $M_s \sim 2.3 \times 10^4$ A/m, and $M_s \sim 2.1 \times 10^4$ A/m at $T = 2$ K, 4 K, and 6 K, respectively, which is typical for ferromagnetic materials. The anisotropy field is temperature dependent: $H_a \sim 3.3 \times 10^3$ A/m, $H_a \sim 1.4 \times 10^3$ A/m, and $H_a \sim 1.3 \times 10^3$ A/m at $T = 2$ K, 4 K, and 6 K, respectively. The estimated saturation magnetization is in a good agreement with $M_s \sim 2.3 \times 10^4$ A/m at $T = 3$ K reported previously for a similar system.[27] The resulting $f_r(H)$ dependencies for the array sample match reasonably $f_r(H)$ for the bar sample at corresponding temperatures leading to the same M_s and H_a.

The above evaluated values of M_s and H_a lead to an unexpectedly high reduced anisotropy field, $H_a/M_s \sim 0.06 - 0.14$. Such a high value, rarely observed in polycrystalline ferromagnetic films with no growth induced anisotropy, cannot be justified by the shape anisotropy only. Indeed, a simple estimation of the shape anisotropy field for a rectangular thin film element[47] of a length a along the applied magnetic field, width b, and thickness c using $H_a/M_s \sim c(\sqrt{4a^2 + b^2} - b)\,/(\pi ab)$ yields $H_a/M_s \sim 5 \times 10^{-4}$ for our bar samples, and $H_a/M_s \to 0$ for a square array sample. This forces one to suggest an internal (microscopic) origin of the high anisotropy field observed in the studied $Pd_{0.99}Fe_{0.01}$ films. Indeed, this could be induced by specific size, shape, and distribution of Fe-rich Pd_3Fe clusters in the Pd-matrix, as well as by the internal anisotropy in Fe-rich clusters. Other direct evidence of the dominance of the internal anisotropy over the shape anisotropy in $Pd_{0.99}Fe_{0.01}$ films resides in matching FMR spectra despite the difference in demagnetizing factors of samples[45,48]

and additional mutual magnetic influence factor of square elements of the array,[49,50] as well as in a close value of the remagnetization width, of the order of $\sim 1.5 \times 10^3$ A/m, for both bar and array samples (compare Figs. 3(a) and 3(b)). These facts support the hypothesis on a cluster nature of the magnetism in $Pd_{0.99}Fe_{0.01}$ films and indicate the absence of FMR dependence on in-plane size, shape, or arrangement of the $Pd_{0.99}Fe_{0.01}$ sample. Within such a cluster picture, the absence of the temperature dependence of the saturation magnetization M_s implies the confinement of the magnetic moments within Fe-rich clusters, while the reduction of H_a with temperature points toward the weakening of the exchange interaction between Fe-rich clusters via the polarized Pd-matrix.

We should note that the cluster nature of the magnetism and large H_a/M_s may hinder the management of magnetic state via the shape anisotropy alone. However, since H_a/M_s is determined partially by deposition conditions it may alter, for instance, if $Pd_{0.99}Fe_{0.01}$ is deposited at different temperatures or in the presence of applied magnetic field. In addition, the state of the entire SFS unit is controlled by the magnetic flux through the junction rather than by the particular magnetic state of the $Pd_{0.99}Fe_{0.01}$ barrier. Hence, the anisotropic response of the SFS can be induced simply by the specific shape of the junction.

While we were not able to evaluate M_s and H_a of thinner film samples performing the FMR measurement, we argue that saturation magnetization is thickness dependent. In Ref. 8 and 10, the saturation magnetization of $Pd_{0.99}Fe_{0.01}$ deposited using the same setup was estimated to be $M_s \simeq 0.96 \times 10^4$ A/m for the 30 nm film at 4.2 K and $M_s \simeq 1.35 \times 10^4$ A/m for the 14 nm film at 1.3 K, respectively, using fluxometry of the Josephson junction with the ferromagnetic interlayer. For these thicknesses of $Pd_{0.99}Fe_{0.01}$, we also expect M_s to show noticeable temperature dependence. Thickness dependence of H_a is not apparent since its origin is not well established. If H_a is purely microstructure defined, one would not expect thickness dependence leading to even stronger reduced anisotropy field H_a/M_s.

Another important characteristic of the magnetization dynamics is a Gilbert damping coefficient α. Gilbert damping torque in magnetic systems introduced into the Landau-Lifschitz equation describes the relaxation of precessing magnetization. The Gilbert damping coefficient can be calculated from the FMR spectra shown in Figs. 3(a) and 3(b) by extracting the frequency bandwidth Δf_r:[34,40] $\alpha \sim \Delta f_r/\gamma\mu_0 M_s$. The coefficient α derived for both types of samples is $\alpha \sim 0.1$, i.e., of the typical value of the damping constant in metallic ferromagnets. It ranges smoothly from $\sim$0.08 at $H < 4 \times 10^3$ A/m up to $\sim$0.13 at $H > 15 \times 10^3$ A/m and does not show a temperature dependence.

V. SUMMARY

Summarizing, in this work the magnetization dynamics of dilute ferromagnetic $Pd_{0.99}Fe_{0.01}$ thin films and microstructures grown on Nb was studied. Several modifications were implemented to a standard FMR experiment resulting in an enhancement of the FMR absorption by one order of magnitude, thus making possible observation and analysis of the FMR absorption spectra of $Pd_{0.99}Fe_{0.01}$ films as thin as 100 nm. In contrast to the classical ferromagnetic Py thin film, the FMR spectrum of the $Pd_{0.99}Fe_{0.01}$ film was found continuous for both types of studied samples—bar and square arrays. Basic magnetic parameters including the anisotropy field, saturation magnetization $M_s \sim 2.1-2.5 \times 10^4$ A/m, and Gilbert damping coefficient $\alpha \sim 0.1$ of $Pd_{0.99}Fe_{0.01}$ were estimated from the FMR spectra. A high anisotropy field was revealed; its temperature dependence along with the weakly temperature dependent saturation magnetization and overall similarity of FMR spectra of bar and array samples imply a cluster nature of the magnetism in $Pd_{0.99}Fe_{0.01}$ thin films. A characteristic time scale for magnetization dynamics in these Pd-Fe films was estimated from FMR spectra to $3-5 \times 10^{-9}$ s. These characteristics make thin Pd-Fe nanostructures suitable for designing fast superconductor-ferromagnet-superconductor memory elements.

ACKNOWLEDGMENTS

Authors acknowledge the Ministry of Education and Science of the Russian Federation in the framework of Increase Competitiveness Program of NUST "MISiS" (research project Nos. K4-2014-080 and K2-2014-025), the Russian Foundation for Basic Research (RFBR) (research project Nos. 16-32-00309, 16-32-60133, 15-02-06743, and 15-52-10045). The STM studies have been supported by Russian Science Foundation project No. 15-12-30030. V.S. and V.R. acknowledge partial support by the Program of Competitive Growth of Kazan Federal University. D.R. acknowledges the support from the French Research Agency (ANR) in the framework of MISTRAL project. Authors acknowledge Dr. P. S. Dzhumaev for SEM study and Professor L. S. Uspenskaya for fruitful discussions.

[1]S. Oh, D. Youm, and M. Beasley, Appl. Phys. Lett. **71**, 2376 (1997).
[2]L. R. Tagirov, Phys. Rev. Lett. **83**, 2058 (1999).
[3]R. Held, J. Xu, A. Schmehl, C. W. Schneider, J. Mannhart, and M. Beasley, Appl. Phys. Lett. **89**, 163509 (2006).
[4]E. C. Gingrich, B. M. Niedzielski, J. A. Glick, Y. Wang, D. L. Miller, R. Loloee, W. P. Pratt, Jr., and N. O. Birge, Nat. Phys. **12**, 564 (2016).
[5]B. Baek, W. H. Rippard, S. P. Benz, S. E. Russek, and P. D. Dresselhaus, Nat. Commun. **5**, 3888 (2014).
[6]M. Weides, M. Kemmler, E. Goldobin, D. Koelle, R. Kleiner, H. Kohlstedt, and A. Buzdin, Appl. Phys. Lett. **89**, 122511 (2006).
[7]A. A. Bannykh, J. Pfeiffer, V. S. Stolyarov, I. E. Batov, V. V. Ryazanov, and M. Weides, Phys. Rev. B **79**, 054501 (2009).
[8]V. V. Bolginov, V. S. Stolyarov, D. S. Sobanin, A. L. Karpovich, and V. V. Ryazanov, JETP Lett. **95**, 366 (2012).
[9]V. V. Ryazanov, V. V. Bolginov, D. S. Sobanin, I. V. Vernik, S. K. Tolpygo, A. M. Kadin, and O. A. Mukhanov, Phys. Procedia **36**, 35 (2012).
[10]I. V. Vernik, V. V. Bol'ginov, S. V. Bakurskiy, A. A. Golubov, M. Y. Kupriyanov, V. V. Ryazanov, and O. Mukhanov, IEEE Trans. Appl. Supercond. **23**, 1701208 (2013).
[11]S. V. Bakurskiy, N. V. Klenov, I. I. Soloviev, V. V. Bol'ginov, V. V. Ryazanov, I. V. Vernik, O. A. Mukhanov, M. Kupriyanov, and A. A. Golubov, Appl. Phys. Lett. **102**, 192603 (2013).
[12]V. V. Ryazanov, Phys. Usp. **42**, 825 (1999).
[13]V. V. Ryazanov, V. A. Oboznov, A. Y. Rusanov, A. V. Veretennikov, A. A. Golubov, and J. Aarts, Phys. Rev. Lett. **86**, 2427 (2001).
[14]K. K. Likharev and V. K. Semenov, IEEE Trans. Appl. Supercond. **1**, 3 (1991).

[15]D. S. Holmes, A. L. Ripple, and M. A. Manheimer, IEEE Trans. Appl. Supercond. **23**, 1701610 (2013).
[16]M. I. Khabipov, D. V. Balashov, F. Maibaum, A. B. Zorin, V. A. Oboznov, V. V. Bolginov, A. N. Rossolenko, and V. V. Ryazanov, Supercond. Sci. Technol. **23**, 045032 (2010).
[17]A. K. Feofanov, V. A. Oboznov, V. V. Bolginov, J. Lisenfeld, S. Poletto, V. V. Ryazanov, A. N. Rossolenko, M. Khabipov, D. Balashov, A. B. Zorin *et al.*, Nat. Phys. **6**, 593 (2010).
[18]N. Lazarides, Phys. Rev. B **69**, 212501 (2004).
[19]H. Susanto, E. Goldobin, D. Koelle, R. Kleiner, and S. A. van Gils, Phys. Rev. B **71**, 174510 (2005).
[20]A. V. Shcherbakova, K. G. Fedorov, K. V. Shulga, V. V. Ryazanov, V. V. Bolginov, V. A. Oboznov, S. V. Egorov, V. O. Shkolnikov, M. J. W., and D. Beckmann, Supercond. Sci. Technol. **28**, 025009 (2015).
[21]E. Goldobin, K. Vogel, O. Crasser, R. Walser, W. P. Schleich, D. Koelle, and R. Kleiner, Phys. Rev. B **72**, 054527 (2005).
[22]G. I. Nieuwenhuys, Adv. Phys. **24**, 515 (1975).
[23]I. Y. Korenblit and E. F. Shender, Zh. Eksp. Teor. Fiz. **62**, 1949 (1972) [SOV. Phys. JETP **35**, 1017 (1972)].
[24]V. A. Andrianov, E. P. Kaminskaya, A. Y. Pentin, V. V. Turovtsev, and V. S. Shpinel, Zh. Eksp. Teor. Fiz. **80**, 2430 (1981) [Sov. Phys. JETP **53**, 1272 (1981)].
[25]C. Büscher, T. Auerswald, E. Scheer, A. Schröder, H. v. Löhneysen, and H. Claus, Phys. Rev. B **46**, 983 (1992).
[26]G. R. Stewart and B. L. Brandt, Phys. Rev. B **28**, 2266 (1983).
[27]L. S. Uspenskaya, A. L. Rakhmanov, L. A. Dorosinskii, S. I. Bozhko, V. S. Stolyarov, and V. V. Bolginov, Mater. Res. Express **1**, 036104 (2014).
[28]T. Herrmannsdiirfer, S. Rehmann, and F. Pobell, J. Low Temp. Phys. **104**, 49 (1996).
[29]M. Ewerlin, B. Pfau, C. M. Günther, S. Schaffert, S. Eisebitt, R. Abrudan, and H. Zabel, J. Phys.: Condens. Matter **25**, 266001 (2013).
[30]C. Nistor, K. Sun, Z. Wang, M. Wu, C. Mathieu, and M. Hadley, Appl. Phys. Lett. **95**, 012504 (2009).
[31]S. Rao, J. Rhensius, A. Bisig, M.-A. Mawass, M. K. M. Weigand, C. S. Bhatia, and H. Yang, Sci. Rep. **5**, 10695 (2015).
[32]D. M. S. Bagguley and J. A. Robertson, J. Phys. F: Metal Phys. **4**, 2282 (1974).
[33]D. Hardison and E. Thompson, J. Phys. Colloq. **32**, C1 (1971).
[34]Y.-C. Chen, D.-S. Hung, Y.-D. Yao, S.-F. Lee, H.-P. Ji, and C. Yu, J. Appl. Phys. **101**, 09C104 (2007).
[35]I. Neudecker, G. Woltersdorf, B. Heinrich, T. Okuno, G. Gubbiotti, and C. Back, J. Magn. Magn. Mater. **307**, 148 (2006).
[36]V. S. Stolyarov, T. Cren, F. Debontridder, C. Brun, I. S. Veshchunov, O. V. Skryabina, A. Y. Rusanov, and D. Roditchev, Appl. Phys. Lett. **104**, 172604 (2014).
[37]B. Heller, K.-H. Speidel, R. Ernst, A. Gohla, U. Grabowy, V. Roth, G. Jakob, F. Hagelberg, J. Gerber, S. Mishra *et al.*, J. Nucl. Instrum Methods Phys. Res. B **142**, 133 (1998).
[38]J. R. Long and R. W. Mattozzi, J. Appl. Phys. **55**, 2359 (1984).
[39]T. Shinohara, T. Sato, T. Taniyama, and I. Nakatani, J. Magn. Magn. Mater. **196–196**, 94 (1999).
[40]S. S. Kalarickal, P. Krivosik, M. Wu, C. E. Patton, M. L. Schneider, P. Kabos, T. J. Silva, and J. P. Nibarger, J. Appl. Phys. **99**, 093909 (2006).
[41]N. Àlvarez, G. Alejandro, J. Gòmeza, E. Goovaerts, and A. Butera, J. Phys. D: Appl. Phys. **46**, 505001 (2013).
[42]F. Giesen, J. Podbielski, T. Korn, M. Steiner, A. van Staa, and D. Grundler, Appl. Phys. Lett. **86**, 112510 (2005).
[43]F. Giesen, J. Podbielski, and D. Grundler, Phys. Rev. B **76**, 014431 (2007).
[44]J. Podbielski, F. Giesen, and D. Grundler, Phys. Rev. B **96**, 167207 (2006).
[45]A. Aharoni, J. Appl. Phys. **83**, 3432 (1998).
[46]A. Aharoni, L. Pust, and M. Kief, J. Appl. Phys. **87**, 6564 (2000).
[47]Y. Li, Y. Lu, and W. E. Bailey, J. Appl. Phys. **113**, 17B506 (2013).
[48]O. Kohmoto, J. Mag. Mag. Mater. **262**, 280 (2003).
[49]E. Liverts, A. Grosz, B. Zadov, M. I. Bichurin, Y. J. Pukinskiy, S. Priya, D. Viehland, and E. Paperno, J. Appl. Phys. **109**, 07D703 (2011).
[50]R. Alvarez-Sanchez, J. L. Costa-Kramer, and F. Briones, J. Mag. Mag. Mater. **307**, 171 (2006).